Atomic Scale Control and Visualization of Topological Quantum Phase Transition in π-conjugated Polymers Driven by Their Length.

*Héctor González-Herrero, Jesús I. Mendieta-Moreno, Shayan Edalatmanesh, José Santos, Nazario Martín, David Écija, Bruno de la Torre, Pavel Jelinek**

Dr. Héctor González-Herrero[+], Shayan Edalatmanesh, Dr. Bruno de la Torre, Prof. Pavel Jelinek.
Regional Centre of Advanced Technologies and Materials, Czech Advanced Technology and Research Institute (CATRIN), Palacký University, 78371 Olomouc, Czech Republic.
E-mail: jelinekp@fzu.cz

Dr. Jesús I. Mendieta-Moreno, Shayan Edalatmanesh, Dr. Bruno de la Torre, Prof. Pavel Jelinek.
Institute of Physics, Czech Academy of Sciences, 162 00 Prague, Czech Republic.

Dr. José Santos, Prof. Nazario Martín.
Department of Organic Chemistry, Faculty of Chemistry, University Complutense of Madrid, 28040 Madrid, Spain

Dr. José Santos, Prof. Nazario Martín, Prof. David Écija
IMDEA-Nanociencia, C/Faraday 9, Ciudad Universitaria de Cantoblanco, 28049 Madrid, Spain,

[+] Present address: Department of Applied Physics, Aalto University, 02150 Espoo, Finland.

Keywords: (π-conjugated polymers, topological quantum phase transition, pseudo Jahn-Teller effect, atomic manipulation, scanning tunneling microscopy, non-contact atomic force microscopy)

Abstract text:

Quantum phase transitions driven by quantum fluctuations are transitions between distinct quantum phases of matter. At present, they are poorly understood and not readily controlled. Here, scanning tunneling microscopy and non-contact atomic force microscopy are used to

explore atomic scale control over quantum phase transitions between two different topological quantum states of a well-defined π-conjugated polymer. The phase transition is driven by a pseudo Jahn-Teller effect that is activated above a certain polymer chain length. In addition, theoretical calculations indicate the presence of long-lasting coherent fluctuations between the polymer's two quantum phases near the phase transition, at finite temperature. This work thus presents a new way of exploring atomic-scale control over quantum phase transitions and indicates that emerging quantum criticality in the vicinity of a quantum phase transition can give rise to new states of organic matter.

1. Introduction.

In general, a phase transition is a process whereby one state of matter is transformed into another, with both states having a distinct internal order characterized by long-range fluctuations extending across the entire system. Classical phase transitions are driven by thermal fluctuations, and are well understood within the frame of Landau-Ginzburg-Wilson theory.[1] However, at zero temperature, where no thermal fluctuations occur, a quantum phase transition (QPT) [2] may occur. A QPT is driven by quantum fluctuations imposed by the uncertainty principle whenever a non-thermal parameter such as the pressure, magnetic field, or chemical composition is modified. [3,4] QPTs have been studied extensively in recent years to better understand the mechanisms that govern them and because of their importance in complex phenomena in solid state physics. [5–7]

Continuous QPTs typically occur in the vicinity of a so-called avoided level crossing (see Figure 1), when the energy difference between the ground state and the lowest excited state diminishes and becomes comparable to quantum fluctuations. In principle, under such circumstances, quantum fluctuations alone can cause a phase transition into a new state of matter even at zero Kelvin. [8,9] Importantly, near the critical point (at finite but very low

temperatures) thermal and quantum fluctuations become equally important, giving rise to the so-called quantum criticality phenomenon. In this quantum critical regime both thermal ($\sim k_B T$) and quantum fluctuations (proportional to the characteristic energy scale Δ -defined as energy difference between the ground and first excited states-) play a significant role breaking the conventional quasiparticle picture of the Fermi liquid theory. [10,11] This leads to unconventional thermodynamic and transport properties observed in this quantum state of matter. Thus, quantum criticality is significant even beyond the quantum critical point at T=0.[5-7] Notably, this exotic quantum state plays significant role in our understanding of e.g. high temperature superconductivity,[12–15] ferroelectricity[16,17] or strange metals featuring non-Fermi liquid behavior.[12] Controlling and understanding QPT is thus a key challenge and objective in contemporary physics due to their complexity and inherent quantum character.[18] It is widely expected that a thorough understanding of QPT will facilitate the design of new quantum materials with remarkable properties.

In particular, it is commonly accepted that Peierls instability manifested in π-conjugated polymers by the bond length alternation and a finite band gap is one of the main obstacles for realization of excitonic superconductivity in organic polymers proposed by W.A. Little. [19] From this perspective, the possibility to design π-conjugated polymers in the quantum critical state may open an alternative route to overcome this problem.

In condensed matter physics, considerable attention has been paid to QPT between phases featuring strongly correlated states of matter with complex spin and charge patterns that frequently give rise to spin and charge density waves (CDW). [20,21] However, the presence of such strongly correlated phases significantly increases the difficulty of studying the phase transition mechanism. Consequently, there is an ongoing search for novel materials in which a QPT occurs between two phases of matter that exhibit only modest correlation and could thus be described well using mean field approximations. In addition, there is a growing interest to

control the proximity to the quantum critical point by precisely tuning material design parameters to enable direct observation of quantum phase transitions.

In one-dimensional π-conjugated polymers, Peierls instability[22] causes alternation of bond lengths between carbon atoms together with variation in the corresponding bond order, which gives rise to π-conjugation.[23,24] The π-conjugation can also be regarded as a CDW phase characterized by Fermi surface nesting and a complex interplay between electronic and lattice degrees of freedom.[25,26] Remarkably, even very simple polymers such as polyacetylene may form distinct quantum topological phases, as demonstrated by the celebrated SSH model,[27] according to which one hallmark of the non-trivial topology of the electronic structure is the presence of in-gap energy edge states.

Recent progress in the field of on-surface synthesis [28,29] supported by high-resolution imaging by scanning probe microscopy [30,31] has enabled the development of new strategies for synthesizing organic hydrocarbon materials with atomistic control [32] and for studying their inherent electronic, magnetic, and topological properties.[33–36] Using such on-surface synthetic protocols, we recently demonstrated that distinct π-conjugation resonance forms and the corresponding topological phases can be tuned in acene-bridged π-conjugated polymers by selecting suitable acene units (i.e., by varying the monomer constituents of the polymers).[37] The change of quantum class from topologically trivial to non-trivial was accompanied by a significant reduction of the electronic band gap and a rearrangement of the π-bonds together with the emergence of zero-energy edge states resulting from the non-trivial topology of the electronic band structure.[38]

Here we show that the length of a 1D polymer can serve as a non-thermal parameter that can be adjusted to induce a topological QPT. This is demonstrated experimentally using pentacene

bridged polymers.[37] In the limit of infinite length, such polymers exist in a topologically non-trivial quantum phase. We used scanning probe microscopy (SPM) and theoretical simulations to systematically study the evolution of the π-conjugated resonance form and level crossing of the frontier orbitals (see schematic depiction in Figure 1) together with the emergence of the edge states with increasing polymer length. Our results show that the topological phase transition is driven by the length of the polymer. This behavior is attributed to a multi-orbital pseudo Jahn-Teller effect [39] resulting from length-dependent vibronic coupling between occupied and unoccupied frontier orbitals. In addition, our density functional theory (DFT) molecular dynamics simulations indicate the presence of long-lived coherent fluctuations at finite temperature between the two distinct π-conjugated/topological phases of the polymers situated near the topological phase transition.

2. Results and discussion.

Pentacene polymers [37,40] were grown by depositing the precursor 4BrPn (6,13-bis(dibromomethylene)-6,13-dihydropentacene) on an Au (111) surface under ultra-high vacuum conditions and subsequent annealing of the surface at 500K. This promotes homocoupling of the 4BrPn molecules, leading to the formation of pentacene polymers. To control the final length of our polymers, we intentionally varied the initial coverage of the precursor molecules. For coverages below 15%, finite polymers were obtained (see Figure S1a-c for representative scanning tunneling microscopy (STM) images of the surface with 4%, 12%, and 15% coverage, and the polymers obtained after annealing). In this way we obtained a wide range of pristine defect-free polymers with lengths in the range from 2 to ~50 monomers.

In a recent previous study,[37] we investigated very long pentacene polymers (with lengths of 50-100 nm) grown on Au (111) that exhibit in-gap edge states due to the non-trivial topology of their electronic band structure. This raises the possibility that the length of a polymer could

influence its topological quantum class. To test this hypothesis, we employed a modified synthetic protocol and discovered that chains with fewer than 26 monomer units lack in-gap edge states. This indicates that pentacene chains only exhibit the non-trivial topology when their length exceeds some critical threshold. Figures 2a and b show high-resolution atomic force microscopy (AFM) and STM images (acquired simultaneously using a CO tip [30]) of two different defect-free chains with 24 and 26 monomers, respectively. We chose these two chain lengths because there is a visible difference in their electronic structure. For example, low bias STM images near the Fermi level (see the STM images at ~3 meV shown in Figures 2a, b) clearly show that the 26 monomers chain features in-gap edge states whereas the 24 monomers chain does not. The in-gap edge state is also visible as a conductance peak around the Fermi energy in the dI/dV spectra acquired at the end of the non-trivial chains (see Figure S2 for an example and ref. 36).

Figure 2c shows selected dI/dV spectra of defect-free polymers of different lengths exhibiting well-defined increases in conductance related to the energies of the HOMO and LUMO orbitals, which determine the polymer's electronic band gap. The evolution of the HOMO/LUMO band gap as function of polymer length is shown in Figure 2d; the band gap of the 1D polymer varies continuously from ~1.2 eV for a dimer chain to ~350meV (resulting from a HOMO energy of -150 meV and a LUMO energy of 200 meV) for the decamer. For longer polymers, the band gap remains constant. However, the saturation of the band gap does not seem to be directly related to the trivial/non-trivial transition of the polymers because the QPT happens at some length between 24 and 26 monomers. Figure 2e shows representative dI/dV maps obtained at the HOMO/LUMO energies of the chains for different topological phases. Interestingly, the features observed for the HOMOs of the trivial polymers are found in the LUMOs of the non-trivial chains and vice versa. Similar behavior was previously observed when comparing the CB and VB of anthracene and pentacene polymers,[37] in which

it causes a change in the Zak phase and thus the topological quantum class.[41] It should be noted that Figure 2d provides direct evidence that an avoided level crossing scheme is associated with a continuous QPT. This indicates that the HOMO/LUMO crossing level plays a decisive role in the topological phase transition, as we will elaborate below.

The change of topological state of these polymers is accompanied by a change in their π-conjugation (i.e., their resonance form), from ethynylene-aromatic (topologically trivial in acene polymers) to cumulene-quinoid (topologically non-trivial in pentacene polymers). This change in the character of the π-conjugation (which can also be considered to represent a transition between two distinct CDW phases) can be directly observed in high-resolution AFM images obtained with CO-functionalized tips. Figure 2f shows two high-resolution AFM images of the central part of the trivial and non-trivial chains in Figures 2a and b, together with profiles along the main axes of each chain (shown as red and blue lines superimposed on the AFM images). The triple bond of the ethynylene link in the topologically trivial chain gives rise to a protrusion in the bridging unit (see the red profile in Figure 2f). Whereas bright protrusions (with corresponding peaks in the red profile) are observed throughout the trivial polymer, these protrusions are absent in the non-trivial chain and the intensity of the peaks decreases upon moving closer to the central part of the chain (see the blue profile in Figure 2f). This indicates a transition from ethynylene-like conjugation in the topologically trivial case to cumulene-like conjugation in the topologically non-trivial polymer.

To enable more precise experimental control over the phase transition in π-conjugated polymers, we developed a novel two-step strategy based on hydrogenation of the pentacene polymers followed by selective removal of the added hydrogen atoms from the desired part of the chain by atomic manipulation using the STM tip.

Exposing pentacene polymers to atomic hydrogen in a UHV chamber leads to the highly selective adsorption of two hydrogen atoms at the 7,12 or the 5,14 positions of the pentacene core (see Figures 3a and b and details of hydrogenation process in the Methods section). Figure 3b presents experimental and theoretical AFM images of the hydrogen defects, which are in excellent agreement. The high site-selectivity of the hydrogen adsorption process is dictated by the formation of a new π-resonance form with two Clar's sextets, which minimizes the total energy of the hydrogenated product (see Figure S3). The hydrogenation process substantially increases the polymer's electronic band gap (to ~1.8 eV; see Figure S4) and creates an ideal template allowing the controlled formation of extended pristine pentacene polymers with different lengths.

The hydrogen pair defects can be removed in a controlled way by placing the STM tip on top of one of them (indicated by the red dot in Figure 3c) and acquiring a distance versus voltage curve, ramping the voltage from 1.5 V to 2.5-3.0 V with a constant current (~10 pA). In the plot in Figure 3c we can observe a sudden jump around 2.5 V, indicating successful removal of the extra hydrogen atoms (see Figure S5 for snapshots of a hydrogen removal process). Repeated application of this protocol enables the selective engineering of regions of pristine pentacene polymers whose topological phase depends on their length. As an example, Figure 3d shows an AFM image of a long fully hydrogenated pentacene polymer before our manipulation experiment, while the AFM image in Figure 3e shows the chain after multiple manipulations (hydrogen removals) featuring a trivial chain consisting of 16 monomers (the left part of the chain) and a non-trivial chain of 31 monomers (right part of the chain). The low bias STM image of the modified polymer shown in Figure 3e reveals the existence of the edge state in the topologically non-trivial part of the chain and its absence in the trivial part. Additionally, dI/dV maps acquired at the HOMO and LUMO energies (-150 meV and 200

meV respectively) show the inversion of the orbitals of the trivial and non-trivial polymers (see the bottom two panels of Figure 3e). Importantly, the artificially formed pentacene polymers exhibit the same behavior as the previously described finite pristine chains. This methodology allowed us to fabricate a 25 monomers chain, which we couldn't locate within the pristine polymers, finding it in a trivial topological state (see Figure S6).

To summarize the experimental observations, the polymer's quantum topological phase transition is accompanied by an avoided level crossing of frontier HOMO/LUMO orbitals and the transformation of the π-conjugation resonance form, as shown schematically in Figure 1. Polymers in the topologically non-trivial phase feature zero-energy edge states due to the bulk-boundary correspondence. Moreover, we also observe a significant renormalization of the electronic band gap for very short chains, but once the polymer length exceeds a certain threshold, the energy band gap remains almost constant even near the phase transition (see Figure 2d).

To better understand the QPT, we performed total energy DFT calculations [42,43] of free-standing pentacene-bridged polymers of various lengths. Figure 4a shows the evolution of the frontier orbital energies of polymers of different lengths, which form the conduction and valence bands in the limit of an infinite polymer. The coloration of the circles representing each frontier orbital indicates their bonding (ψ^b, red) or antibonding (ψ^a, blue) character at the triple bond of the bridging unit (see Figure 1). According to the calculations, the phase transition occurs when the polymer length increases from 10 to 11 units and is indicated by the emergence of in-gap edge states (represented by black dots in Figure 4a) and the unification of the bonding (red) and antibonding (blue) character of the empty and occupied states, respectively.

The spin-restricted DFT calculations reproduced most of the experimental observations including (i) the occurrence of the phase transition accompanied by the avoided level crossing of the frontier orbitals (see Figure 4a), (ii) the transformation of the π-conjugation at a certain critical length (Figure 4a), and (iii) the emergence of in-gap energy edge states characteristic of the topologically non-trivial phase (see Figure S7). In addition, calculated d*I*/d*V* images [44] of single particle frontier HOMO/LUMO orbitals agreed extremely well with the experimental data presented in Figure 2e. The only discrepancy we note is that the polymer length threshold for the formation of the topologically non-trivial phase (~11 monomer units) is shorter than was observed experimentally (~26 monomer units). This deviation can be attributed to limited precision of single particle DFT calculations. Namely, the precise threshold for the transition depends on the choice of exchange-correlation functional, see Table S1. The comparison reveals the dependence of the critical length on the calculated HOMO-LUMO band gap. As the electronic band gap is one of the key factors determining the strength of the vibronic coupling (see denominator of Equation 1), the well-known underestimation of the band gap by DFT causes a systematic overestimation of the vibronic coupling. Consequently, they yield that the transition happens at shorter longitudes than in the experiment. Furthermore, the second source of the inaccuracy in the calculations stems from the vibronic matrix element (see numerator in Equation 1), which couples the ground and excited states via a selected vibrational mode. As the DFT method is a single determinant theory formulated for the ground states, it is not surprising that these values are overestimated as well. Besides that, we should not forget that our calculations are performed for free-standing chains without the presence of metallic substrate, which may impose an additional source of inaccuracy. Despite this minor deficiency, we believe that the DFT calculations provide a reliable qualitative description of the mechanism governing the phase transition.

Interestingly, the frontier electronic orbitals involved in the avoided level crossing have opposing bonding/antibonding characters at the triple bond (see Figures 1 and 4b). Therefore, the level crossing is directly associated with the weakening and elongation/stretching of the triple bond observed during the phase transition, which is driven by the occupancy of anti/bonding frontier orbitals. This suggests that phonon softening may be responsible for the phase transition. Spontaneous symmetry breaking in molecular systems with nondegenerate electronic states is often caused by a pseudo Jahn-Teller mechanism [39] driven by vibronic coupling of low-lying excited states to vibrational modes of specific symmetries to establish a new ground state at zero temperature. We will show that a pseudo Jahn-Teller effect is indeed responsible for the phase transition in the pentacene polymers.

The total vibronic coupling γ_Q^{tot} corresponding to a given soft phonon mode Q, which is a source of the phonon softening of the system, is equal to the sum of the individual vibronic couplings γ_Q^{ij} between pairs of frontier orbitals:

$$\gamma_Q^{ij} \sim \frac{\langle \psi_i | \partial H/\partial Q | \psi_j \rangle}{E_j - E_i} \quad \text{Equation (1)}$$

Here, ψ_i, ψ_j, E_i, E_j are the wavefunctions and eigenenergies of the i-th occupied and j-th unoccupied electronic states, respectively. The numerator $\langle \psi_i | \, \partial H/\partial Q \, | \psi_j \rangle$ represents the off-diagonal vibronic coupling constant [39] between the occupied and unoccupied electronic states mediated by vibrational mode Q. The presence of the energy difference $E_j - E_i$ in the denominator has two important consequences: (i) only low-energy excitation electronic states contribute significantly to the vibronic coupling; and (ii) vibronic coupling is enhanced as the band gap diminishes. The second consequence is often considered decisive in most spontaneous symmetry breaking processes. However, this argument cannot be fully applied to

our system because the experimental band gap remains almost constant near the critical point, as shown in Figure 2d.

Our findings thus suggest that the numerator in Equation 1 plays a decisive role in the phase transition. To understand its role, we analyzed a pentacene dimer to identify potentially relevant couplings between vibrational modes and frontier orbitals involved in the pseudo Jahn-Teller effect [39,45]. Our calculations show that the two highest occupied frontier orbitals (HOMO-1 and HOMO) have opposing bonding (ψ^b) and antibonding (ψ^a) characters at the triple bond of the bridging unit, and that the same is true for the two lowest frontier unoccupied orbitals (LUMO and LUMO+1), as shown in Figure 4b.

Moreover, we found that an in-plane stretching vibrational mode Q of the triple bond in the bridging unit (see inset of Figure 4c) has a symmetry that allows for significant vibronic coupling between frontier electronic orbitals with the same bonding (ψ^b) or antibonding (ψ^a) symmetry. This coupling is substantially weaker between frontier orbitals of opposing symmetry. In the case of the dimer chain shown in Figure 4b, we found that the vibronic coupling between orbitals of the same symmetry mediated by the stretching vibrational mode Q is $\gamma_Q^{b,b} = \gamma_Q^{a,a}$= 0.73 eV/Å whereas it vanishes for orbitals of different symmetries ($\gamma_Q^{a,b} \sim 10^{-3}$). Tables S2-S4 summarize the calculated vibronic couplings between occupied and unoccupied frontier orbitals for dimer, trimer, and pentamer chains, showing that the sum of the couplings increases with the chain length. Thus, the longer the polymer chain, the greater the number of electronic states belonging to the emerging valence and conduction bands (see Figure 4a). Additionally, the number of stretching vibrational modes Q of the bridge unit (see Figures S8, S9) increases linearly with chain length. Consequently, the

strength of the vibronic coupling increases steadily with chain length (as shown in Figure 4c) until it reaches a critical value and the system undergoes a phase transition.

The phase transition from topologically trivial to non-trivial is accompanied by the crossing of HOMO and LUMO frontier orbitals with different bonding characters. This level crossing causes the set of orbitals forming the valence band to have the same antibonding character at the triple bond, whereas the conduction band is formed exclusively from wavefunctions with the same bonding character at the triple bond (see Figures 4a, b and Figures S7, S10-11). Consequently, the vibronic coupling via the stretching mode vanishes. As the occupied orbitals of the valence band have antibonding symmetry, the triple bond is weakened, causing the topological transformation to be accompanied by a transformation of the system's π-conjugation type from ethynylene-aromatic to cumulene-quinoid. Our analysis shows that systems with conduction and valence bands consisting of mixtures of wavefunctions with different symmetries are more prone to vibronic instability. We believe that this paradigm may extend to other π-conjugated systems such as acenes and graphene nanoribbons.[46]

Figure S7 shows the real-space wavefunctions of a 15-unit pentacene polymer, found in a topologically non-trivial phase featuring in-gap edge states. Interestingly, we observe that the exchange of the bonding ψ^b and antibonding ψ^a orbitals are localized mostly in the central part of the polymer, while at the edges the frontier orbitals retain the "original" electronic character seen in short topologically trivial polymers. This finding agrees well with the experimental data on topologically non-trivial polymers (see Figure S12): high-resolution AFM images and reverse contrast dI/dV maps of the HOMO/LUMO show that the triple bonding character of the bridge units is retained to a large degree at the ends of the polymers but not in its central part (see Figure 3e).

The occurrence of QPT at finite temperatures gives rise to quantum criticality, which is the subject of intense ongoing research because it represents an exotic state of matter. The results presented herein suggest that quantum criticality may emerge in pentacene-bridged polymers. Therefore, to investigate the behavior of polymers exceeding the critical length threshold at elevated temperatures, we performed QM/MM MD simulations [43,47] of polymers with 15 monomer units (QM region) on an Au (111) substrate (MD region) at 100 Kelvin (for details, see the Methods section). Interestingly, we observe cyclic reappearance of the in-gap edge states ψ^e (black) accompanied by energy level crossing of the bonding ψ^b (red) and antibonding ψ^a (blue) frontier orbitals, as shown in Figure 4d and movie S1. This indicates that the polymer fluctuates continuously between the two topological phases at finite temperature. These fluctuations are driven by the presence of a new stable vibrational mode with an oscillation period of ~1ps. This vibrational mode resembles a breathing mode that causes the total length of the polymer to vary continually. Both the level crossing and the cyclic reappearance of the edge state are completely absent in MD simulations of a topologically trivial chain with only 5 monomer units (see Figure S13). While we recognize the inability of current DFT methods to properly describe electronic structure, we believe that the coherent emergence of two distinct topological phases on a timescale of at least tens of picoseconds is consistent with the existence of the quantum criticality in π-conjugated polymers whose lengths place them near the topological phase transition.

We believe that these findings will motivate further research into quantum criticality in polyacenes and related systems using appropriate experimental techniques. Unfortunately, the evolution of such quantum coherence cannot be studied directly by low-temperature microscopy because its spatial and energy resolution are both greatly reduced at elevated temperatures. However, it may be possible to study the potential critical behavior of these

polymers at finite temperature by measuring the conductance through single chains [48,49] near the quantum phase transition.

3. Conclusions.

In conclusion, we have demonstrated the length dependence of the quantum topological phase of pentacene polymers. We showed that once the critical length has been reached (~ 26 monomers), the polymers undergo the quantum phase transition from a trivial to a non-trivial topology. The transition is accompanied by an avoided level crossing of the frontier orbitals together with a change in the π-conjugation of the polymer. Our DFT calculations mimic the experimental results and identify a pseudo Jan-Teller as the driving mechanism.

In addition, we present a novel strategy based on hydrogenation and atomic manipulation which provides a way of engineering topological heterostructures with sub-nanometer precision. This hydrogenation protocol could be transferred to an industrial environment as long as a vacuum environment with an atomic hydrogen source is available. We show the control to create conjoining polymer segments with different topological phases, or two separated segments with the same topology. This provides a playground enabling investigation of quantum phenomena emerging from the interfaces between trivial and non-trivial phases as well as the interaction of two topologically protected edge states and their protection from disorder or external stimuli.

We anticipate that the behavior documented herein may give rise to a fluctuating quasi-metallic entangled phase within the polymer. We envision that these observations will stimulate more elaborate studies on the electronic structure of π-conjugated polymers, the effect of their geometric dimensions on their topological quantum class, and the emergence of complex quantum ground states in the quantum criticality regime.

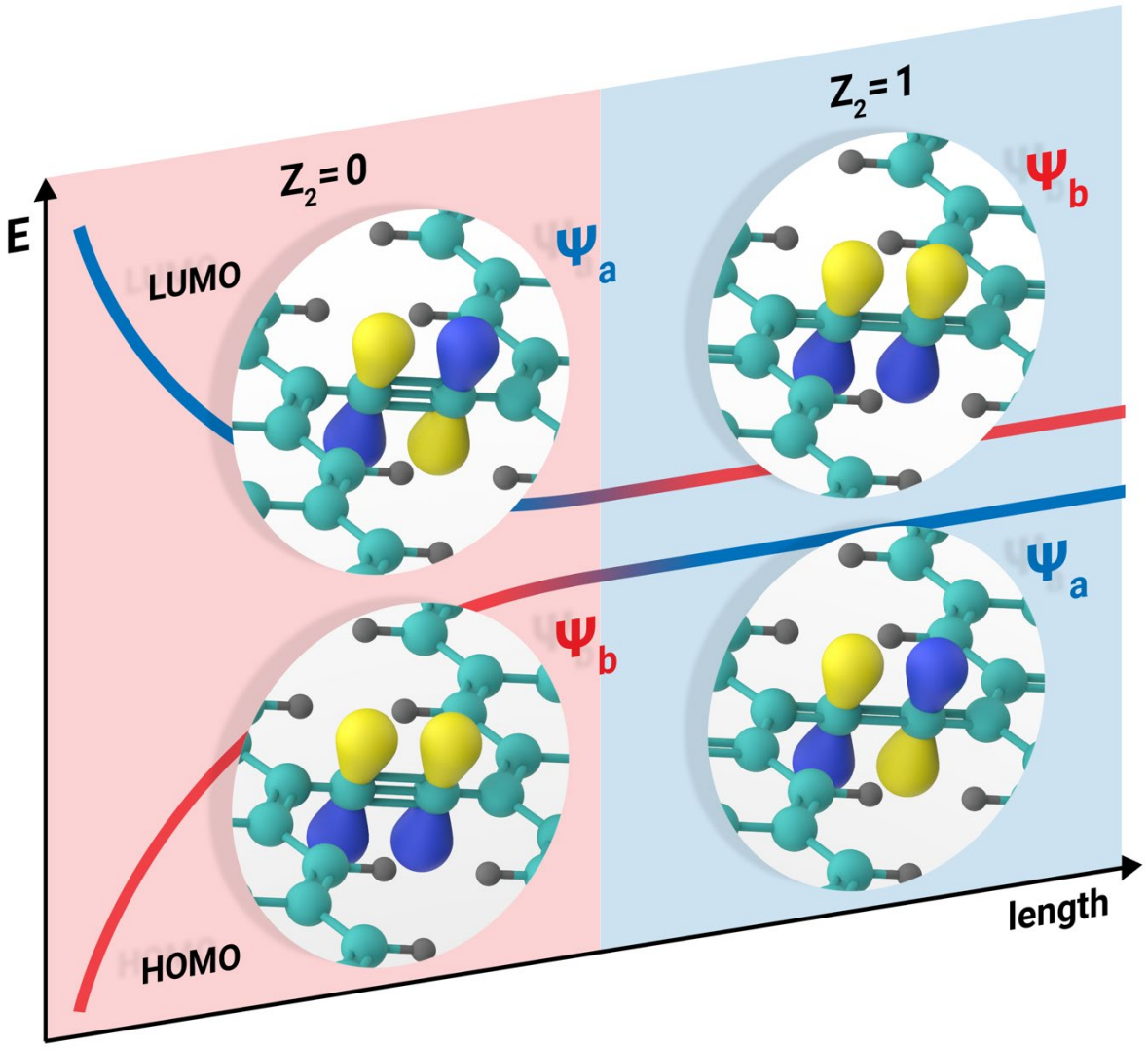

Figure 1. Schematic depiction of the length-dependent topological quantum phase transition in π-conjugated pentacene bridged polymers. The phase transition is driven by an avoided level crossing of two frontier HOMO/LUMO π-orbitals with distinct bonding (ψ^b) and antibonding (ψ^a) characters at the two carbon atoms forming the bridge. This exchange of two frontier bonding ψ^b and antibonding ψ^a orbitals in the avoided level crossing weakens the triple bond in the bridge, causing a transformation of the π-resonant form of the polymer and the emergence of the in-gap edge states characteristic of the topologically nontrivial quantum phase.

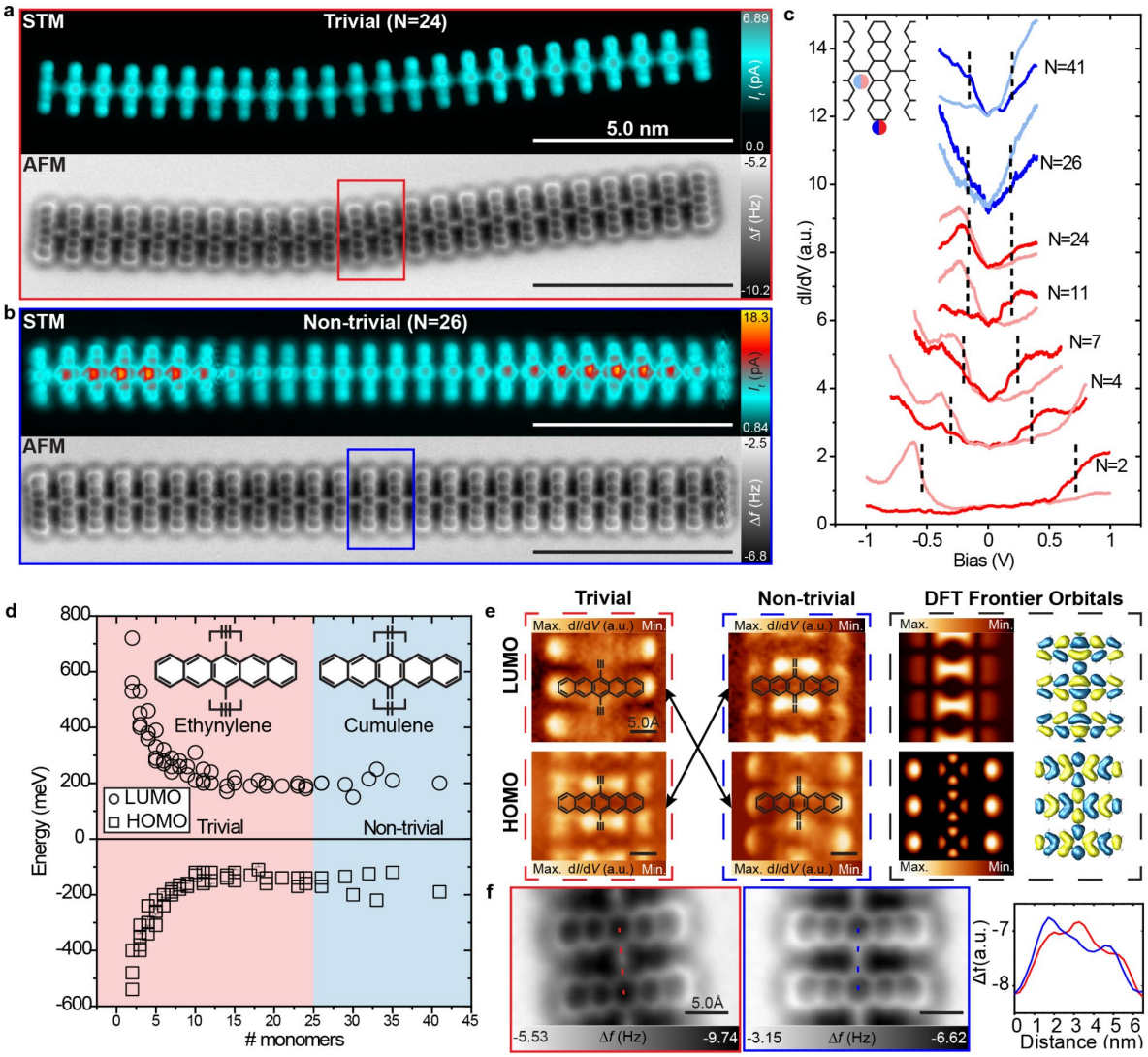

Figure 2. Characterization of the length-dependence of pentacene polymers. a) Constant height STM (top) and nc-AFM (bottom) image of a 24 monomers pentacene. b) Constant height STM (top) and nc-AFM (bottom) image of a 26 monomers pentacene. c) d*I*/d*V* spectra of polymers of different lengths. Results for topologically trivial and non-trivial chains are plotted in red and blue, respectively. Inset: schematic view showing the positions at which the d*I*/d*V* curves were acquired within a pentacene unit in the central part of the polymer. d) Evolution of the HOMO and LUMO energies with the polymer length. e) Experimental d*I*/d*V* maps of the LUMO (top) and HOMO (bottom) of trivial and non-trivial chains (left and center, respectively). Simulated d*I*/d*V* maps of the frontier orbitals (right) of the infinite pentacene bridged chain. f) Expansion of the regions enclosed in the red/blue rectangles in the

AFM images from panels (a-b) and height profiles along the red and blue lines shown in the expansions. The red profile features a peak corresponding to a bright spot in the AFM image that is associated with the triple bond of the bridge unit. This peak is absent in the blue profile, indicating that the two carbon atoms are linked by a double bond in this case.

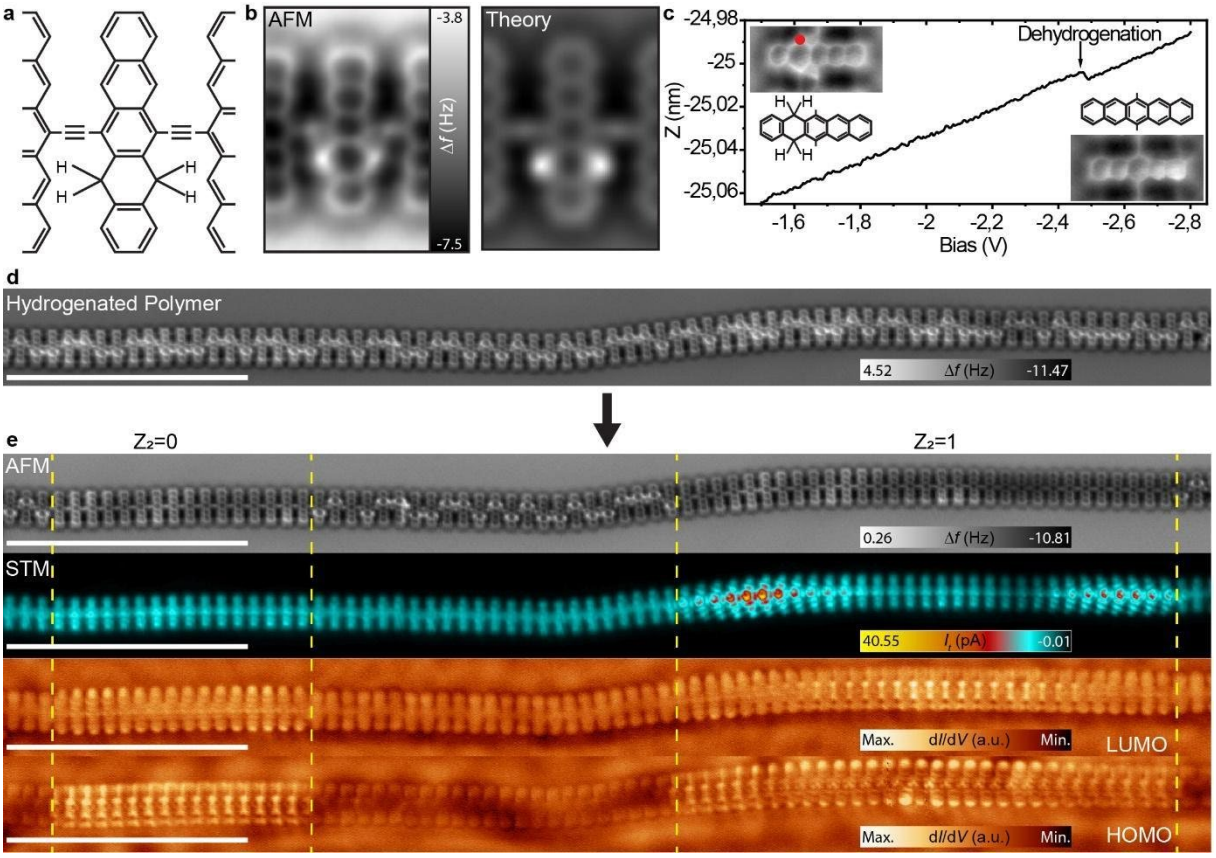

Figure 3. Engineering pentacene polymers by tip-induced dehydrogenation. a) Chemical structure of a hydrogenated pentacene polymer. b) Experimental (left) and simulated (right) AFM images of the hydrogenated pentacene polymer. c) Characteristic distance vs. bias curve acquired at the position indicated by the red dot, showing the removal of the two "extra" hydrogens from the pentacene unit. Top left inset: nc-AFM image of the pentacene unit before the curve was recorded and the corresponding chemical structure. Bottom right inset: nc-AFM image after removing the two extra hydrogens and the corresponding chemical structure. d) nc-AFM image of a fully hydrogenated pentacene polymer. e) From top to bottom: nc-AFM image of the chain shown in panel (d) after the hydrogen manipulations at two distinct parts

of the polymer to produce short topologically trivial (left) and long topologically non-trivial (right) polymer segments; low bias STM image of the polymer chain; LUMO and HOMO dI/dV maps of the engineered polymer revealing the exchange of frontier orbitals between topologically trivial and non-trivial segments of the polymer. Dashed yellow lines were added to guide the eye.

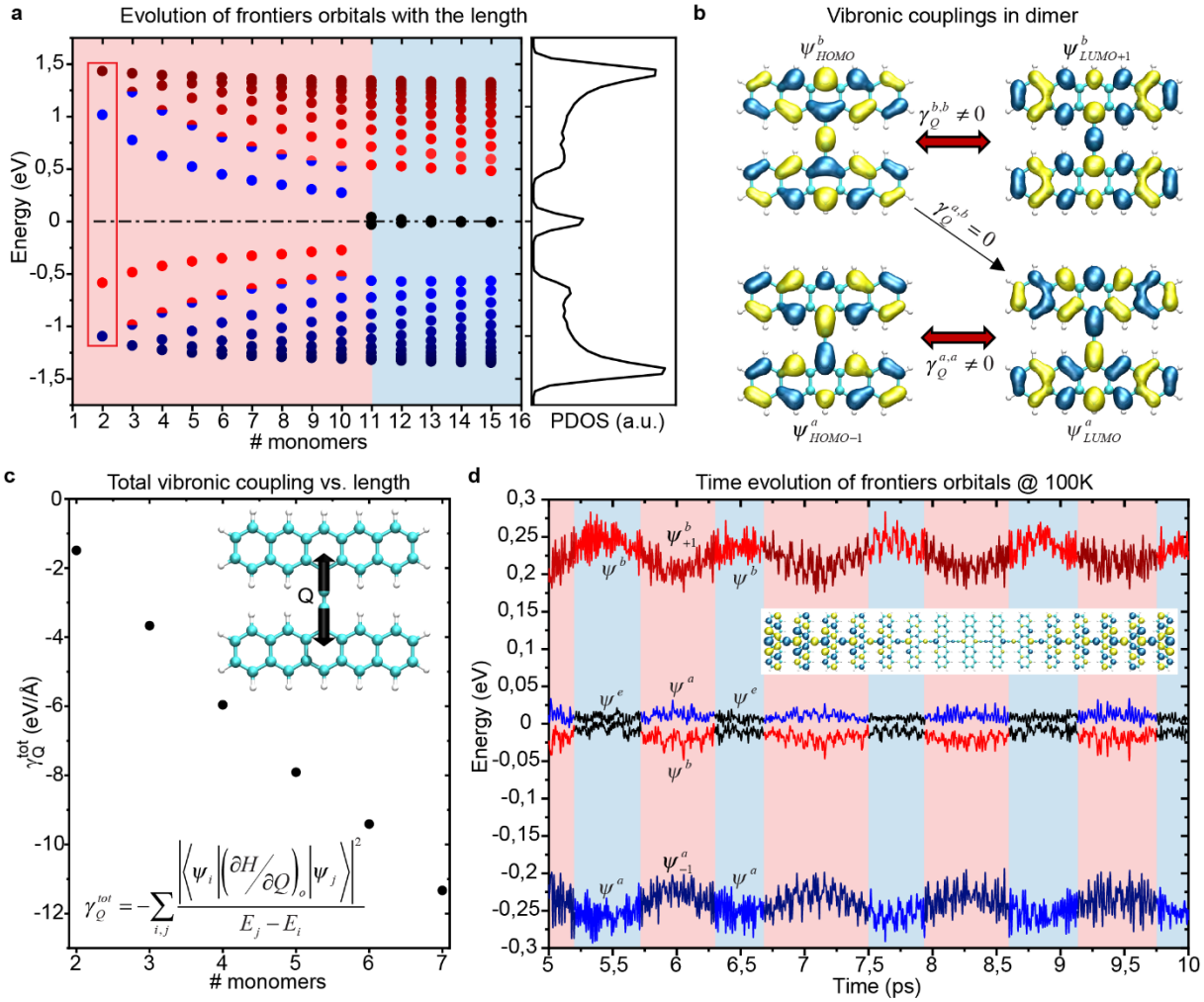

Figure 4. Theoretical simulations of electronic states and vibronic couplings of pentacene bridged polymers. a) Calculated electronic spectra of the frontier orbitals of pentacene polymers with different numbers of monomers together with the projected density of states (right) for an infinite polymer. The colors of the circles indicate the bonding (ψ^b, red) or antibonding (ψ^a, blue) character of the corresponding frontier orbital at the triple bond of the

bridging unit; black circles represent the in-gap edge states emerging in the topologically non-trivial quantum phase. b) The two highest occupied (left) and lowest unoccupied (right) frontier orbitals of the dimer (see box in (a)), which have different bonding ψ^b and antibonding ψ^a characters at the bridging unit and thus different strengths of vibronic coupling between orbitals of different bonding character such that $\gamma_Q^{b,b} = \gamma_Q^{a,a} \neq 0$ and $\gamma_Q^{a,b} \sim 0$ (see table S1). The strength of vibronic coupling between frontier orbitals is represented schematically by the thickness of the arrows between the different orbitals. c) Evolution of the total vibronic coupling γ_Q^{tot} with the length of the polymer. The inset shows the in-plane stretching vibrational mode that mediates vibronic coupling between frontier orbitals. d) Time evolution of selected electronic states of a 15-unit polymer at 100 Kelvin showing the reappearance of the in-gap edge states ψ^e (black) accompanied by energy level crossing of the bonding ψ^a (red) and antibonding ψ^b (blue) frontier orbitals. The inset shows the electronic wavefunction of the in-gap edge state.

4. Methods

Experiments

All experiments were conducted in an ultra-high vacuum chamber hosting a low temperature (4.2 K) STM/AFM (Createc). A bias voltage was applied to the sample and the base pressure was ~5.0 E-10 mbar.

STM/AFM images were acquired with a Pt/Ir tip mounted on a qPlus sensor (resonant frequency of ~30 kHz; stiffness of ~1,800 N m–1), cut and sharpened with a focused ion beam. High resolution nc-AFM images were obtained at constant height, operating the qPlus sensor in the frequency modulation mode using a constant amplitude oscillation of 50 pm. The metal tip apex was prepared by gentle indentation (~ 1 nm) on the clean Au (111) substrate and functionalized with a CO molecule dosed at low temperature.

Conductance d*I*/d*V* spectra and maps were acquired using a lock-in technique, with an ac voltage (frequency: 700-800 Hz, amplitude: 1-10 mV rms) added to the dc sample bias. d*I*/d*V* maps were recorded in constant current mode.

All data were processed using the WSxM software.[50] All presented images and spectroscopic plots represent raw data with only slope and gaussian corrections.

The Au (111) substrate was prepared by standard cycles of Ar^+ sputtering at energies from 1.0 to 1.5 kV followed by annealing at 800 K.

The 4BrPn molecules were deposited from a tantalum crucible at ~450 K on the freshly cleaned Au (111) crystal held at RT and subsequently annealed up to 500 K to induce on-surface polymerization

Hydrogenation of the pentacene polymers was achieved by removing the sample from the cryostat and increasing the partial pressure of molecular hydrogen in the STM chamber while keeping a Bayard-Alpert ion gauge filament on (Granville-Phillips® Series 274). The molecular hydrogen in the residual gas was then cracked by the filament and adsorbed by our polymers. No chain hydrogenation occurred in control experiments in which the polymer-decorated sample was left in the UHV chamber with the ion gauge off even after extended periods of time.

Theory

Our QM/MM simulations were performed using Fireball/Amber method, [47] which combines an interface force field [51] for the Au surface with Fireball local orbital DFT [43] for the molecule. Spin-restricted Fireball calculations used the BLYP exchange-correlation functional [52,53] with D3 corrections [54] and norm-conserving pseudopotentials, using a basis set of optimized numerical atomic-like orbitals with cut off radii for H (s=5.42 a.u.) and C (s,p=5.95 a.u.).[55] The QM/MM MD simulation for the 5-, 15-, and 20-unit chains were performed at 100K with a Langevin thermostat for 10 ps with a time step of 0.5 fs with a velocity Verlet middle propagation scheme and Born-Oppenheimer approximation. For the colors criteria of

the MD simulation (Figure 4d) we use the length of the polymer that is correlated with the band gap, see Movie S1. Vibronic couplings were calculated using a previously reported formalism for calculating non-adiabatic couplings with a numerical local basis set [45] using the Fireball code.

For all free-standing finite and infinite chains, spin-restricted DFT calculations were done using Fireball code with the parameters described above. We also obtained very similar results using FHI-AIMS, [42] in which geometry optimizations and electronic structure analyses were performed using the B3LYP [56] exchange–correlation functional. Systems were allowed to relax until the remaining atomic forces fell below 10-2 eV $Å^{-1}$. To sample the Brillouin zone for the infinite system with periodic boundary condition, a Monkhorst–Pack grid of 18 × 1 × 1 was used. For the finite systems, one k-point at the Gamma point was used. Theoretical dI/dV maps were calculated from the electronic structure obtained using the Fireball DFT [43] package and with Probe Particle Scanning Probe Microscopy (PP-SPM) code for an s-like orbital tip. [44,57] The AFM simulations of the hydrogenated pentacene were performed using PP-SPM code with a DFT-relaxed atomic structure.

Supporting Information

Supporting Information is available from the Wiley Online Library or the author.

Acknowledgements

This work was supported by Praemium Academie of the Academy of Science of the Czech Republic, GACR 20-13692X (P.J.). We acknowledge financial support from Comunidad de Madrid [project QUIMTRONIC-CM (Y2018/NMT-4783)], Ministerio de Ciencia e Innovación (#PID2019-108532GB-I00) and Severo Ochoa Programme for Centers of Excellence in R&D (MINECO, grant SEV-2016-0686).

Received: ((will be filled in by the editorial staff))
Revised: ((will be filled in by the editorial staff))
Published online: ((will be filled in by the editorial staff))

References

[1] S. Singh, W. J. Jones, W. Siebrand, B. P. Stoicheff, W. G. Schneider, J. Chem. Phys. **1965**, 42, 330.

[2] J. A. Hertz, Phys. Rev. B **1976**, 14, 1165.

[3] H. v. Löhneysen, T. Pietrus, G. Portisch, H. G. Schlager, A. Schröder, M. Sieck, T. Trappmann, Phys. Rev. Lett. **1994**, 72, 3262.

[4] S. A. Grigera, Science (80-.). **2001**, 294, 329.

[5] P. Coleman, A. J. Schofield, Nature **2005**, 433, 226.

[6] S. Sachdev, B. Keimer, Phys. Today **2011**, 64, 29.

[7] R. B. Laughlin, G. G. Lonzarich, P. Monthoux, D. Pines, Adv. Phys. **2001**, 50, 361.

[8] S. Sachdev, Phys. World **1999**, 12, 33.

[9] M. Vojta, Reports Prog. Phys. **2003**, 66, 2069.

[10] Q. Si, S. Rabello, K. Ingersent, J. L. Smith, Nature **2001**, 413, 804.

[11] P. Gegenwart, Q. Si, F. Steglich, Nat. Phys. **2008**, 4, 186.

[12] D. M. Broun, Nat. Phys. **2008**, 4, 170.

[13] S. Nakatsuji, K. Kuga, Y. Machida, T. Tayama, T. Sakakibara, Y. Karaki, H. Ishimoto, S. Yonezawa, Y. Maeno, E. Pearson, G. G. Lonzarich, L. Balicas, H. Lee, Z. Fisk, Nat. Phys. **2008**, 4, 603.

[14] M. P. Allan, F. Massee, D. K. Morr, J. Van Dyke, A. W. Rost, A. P. Mackenzie, C. Petrovic, J. C. Davis, Nat. Phys. **2013**, 9, 468.

[15] B. B. Zhou, S. Misra, E. H. da Silva Neto, P. Aynajian, R. E. Baumbach, J. D. Thompson, E. D. Bauer, A. Yazdani, Nat. Phys. **2013**, 9, 682.

[16] S. E. Rowley, L. J. Spalek, R. P. Smith, M. P. M. Dean, M. Itoh, J. F. Scott, G. G. Lonzarich, S. S. Saxena, Nat. Phys. **2014**, 10, 367.

[17] A. Narayan, A. Cano, A. V Balatsky, N. A. Spaldin, Nat. Mater. **2018**, 18, 223.

[18] S. Mukhopadhyay, R. Sharma, C. K. Kim, S. D. Edkins, M. H. Hamidian, H. Eisaki, S.-I. Uchida, E.-A. Kim, M. J. Lawler, A. P. Mackenzie, J. C. S. Davis, K. Fujita, Proc. Natl. Acad. Sci. U. S. A. **2019**, 116, 13249.

[19] W. A. Little, *Phys. Rev.* **1964**, *134*, A1416.

[20] M. H. Hamidian, S. D. Edkins, S. H. Joo, A. Kostin, H. Eisaki, S. Uchida, M. J. Lawler, E.-A. Kim, A. P. Mackenzie, K. Fujita, J. Lee, J. C. S. Davis, Nature **2016**, 532, 343.

[21] Z. Du, H. Li, S. H. Joo, E. P. Donoway, J. Lee, J. C. S. Davis, G. Gu, P. D. Johnson, K. Fujita, Nature **2020**, 580, 65.

[22] P. Cao, P. Bai, A. A. Omrani, Y. Xiao, K. L. Meaker, H.-Z. Tsai, A. Yan, H. S. Jung, R. Khajeh, G. F. Rodgers, Y. Kim, A. S. Aikawa, M. A. Kolaczkowski, Y. Liu, A. Zettl, K. Xu, M. F. Crommie, T. Xu, Adv. Mater. **2017**, 29, 1701536.

[23] M. Kertesz, C. H. Choi, S. Yang, Chem. Rev. **2005**, 105, 3448.

[24] W. Barford, Electron. Opt. Prop. Conjug. Polym. **2013**, 192.

[25] X. Zhu, J. Guo, J. Zhang, E. W. Plummer, Adv. Phys. X **2017**, 2, 622.

[26] J.-P. Pouget, Comptes Rendus Phys. **2016**, 17, 332.

[27] A. J. Heeger, S. Kivelson, J. R. Schrieffer, W.-P. Su, Rev. Mod. Phys. **1988**, 60, 781.

[28] S. Clair, D. G. de Oteyza, Chem. Rev. **2019**, 119, 4717.

[29] L. Grill, M. Dyer, L. Lafferentz, M. Persson, M. V Peters, S. Hecht, Nat. Nanotechnol. **2007**, 2, 687.

[30] L. Gross, F. Mohn, N. Moll, P. Liljeroth, G. Meyer, Science (80-.). **2009**, 325, 1110.

[31] P. Jelínek, J. Phys. Condens. Matter **2017**, 29, 343002.

[32] D. G. de Oteyza, P. Gorman, Y.-C. Chen, S. Wickenburg, A. Riss, D. J. Mowbray, G. Etkin, Z. Pedramrazi, H.-Z. Tsai, A. Rubio, M. F. Crommie, F. R. Fischer, Science (80-.). **2013**, 340, 1434.

[33] D. J. Rizzo, G. Veber, T. Cao, C. Bronner, T. Chen, F. Zhao, H. Rodriguez, S. G. Louie, M. F. Crommie, F. R. Fischer, Nature **2018**, 560, 204.

[34] O. Gröning, S. Wang, X. Yao, C. A. Pignedoli, G. Borin Barin, C. Daniels, A. Cupo, V. Meunier, X. Feng, A. Narita, K. Müllen, P. Ruffieux, R. Fasel, Nature **2018**, 560, 209.

[35] J. Li, S. Sanz, M. Corso, D. J. Choi, D. Peña, T. Frederiksen, J. I. Pascual, Nat. Commun. **2019**, 10, 200.

[36] N. Pavliček, A. Mistry, Z. Majzik, N. Moll, G. Meyer, D. J. Fox, L. Gross, Nat. Nanotechnol. **2017**, 12, 308.

[37] B. Cirera, A. Sánchez-Grande, B. de la Torre, J. Santos, S. Edalatmanesh, E. Rodríguez-Sánchez, K. Lauwaet, B. Mallada, R. Zbořil, R. Miranda, O. Gröning, P. Jelínek, N. Martín, D. Ecija, Nat. Nanotechnol. **2020**, 15, 437.

[38] J. K. Asbóth, L. Oroszlány, A. Pályi, Lect. Notes Phys. **2016**.

[39] I. B. Bersuker, Chem. Rev. **2013**, 113, 1351.

[40] A. Sánchez-Grande, B. de la Torre, J. Santos, B. Cirera, K. Lauwaet, T. Chutora, S. Edalatmanesh, P. Mutombo, J. Rosen, R. Zbořil, R. Miranda, J. Björk, P. Jelínek, N. Martín, D. Écija, Angew. Chem. Int. Ed. Engl. **2019**, 58, 6559.

[41] J. Zak, Phys. Rev. Lett. **1989**, 62, 2747.

[42] V. Blum, R. Gehrke, F. Hanke, P. Havu, V. Havu, X. Ren, K. Reuter, M. Scheffler, Comput. Phys. Commun. **2009**, 180, 2175.

[43] J. P. Lewis, P. Jelínek, J. Ortega, A. A. Demkov, D. G. Trabada, B. Haycock, H. Wang, G. Adams, J. K. Tomfohr, E. Abad, H. Wang, D. A. Drabold, Phys. status solidi **2011**, 248, 1989.

[44] O. Krejčí, P. Hapala, M. Ondráček, P. Jelínek, Phys. Rev. B **2017**, 95.

[45] E. Abad, J. P. Lewis, V. Zobač, P. Hapala, P. Jelínek, J. Ortega, J. Chem. Phys. **2013**, 138, 154106.

[46] P. Ruffieux, S. Wang, B. Yang, C. Sánchez-Sánchez, J. Liu, T. Dienel, L. Talirz, P. Shinde, C. A. Pignedoli, D. Passerone, T. Dumslaff, X. Feng, K. Müllen, R. Fasel, Nature **2016**, 531, 489.

[47] J. I. Mendieta-Moreno, R. C. Walker, J. P. Lewis, P. Gómez-Puertas, J. Mendieta, J. Ortega, J. Chem. Theory Comput. **2014**, 10, 2185.

[48] P. Gehring, J. M. Thijssen, H. S. J. van der Zant, Nat. Rev. Phys. **2019**, 1, 381.

[49] F. Evers, R. Korytár, S. Tewari, J. M. van Ruitenbeek, Rev. Mod. Phys. **2020**, 92.

[50] I. Horcas, R. Fernández, J. M. Gómez-Rodríguez, J. Colchero, J. Gómez-Herrero, A. M. Baro, Rev. Sci. Instrum. **2007**, 78, 13705.

[51] H. Heinz, T.-J. Lin, R. Kishore Mishra, F. S. Emami, Langmuir **2013**, 29, 1754.

[52] A. D. Becke, Phys. Rev. A **1988**, 38, 3098.

[53] C. Lee, W. Yang, R. G. Parr, Phys. Rev. B **1988**, 37, 785.

[54] S. Grimme, S. Ehrlich, L. Goerigk, J. Comput. Chem. **2011**, 32, 1456.

[55] M. A. Basanta, Y. J. Dappe, P. Jelínek, J. Ortega, Comput. Mater. Sci. **2007**, 39, 759.

[56] A. D. Becke, J. Chem. Phys. **1993**, 98, 5648.

[57] P. Hapala, G. Kichin, C. Wagner, F. S. Tautz, R. Temirov, P. Jelínek, Phys. Rev. B **2014**, 90.

H. González-Herrero, J. Mendieta-Moreno, S. Edalatmanesh, J. Santos, N. Martín, D. Écija, B. de la Torre, P. Jelinek*

Title

Atomic scale control and visualization of topological quantum phase transition in π-conjugated polymers driven by their length

ToC figure

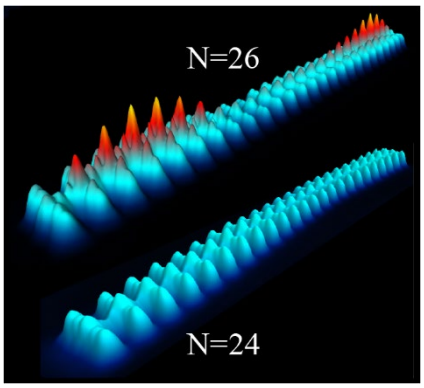

Length control of π-conjugated pentacene polymers leads to the observation of a topological quantum phase transition. The transition is marked by the emergence of a zero energy in-gap edge state. Pseudo Jan-Teller effect is identified as the driving mechanism by our theoretical calculations. Furthermore, atomic manipulation with STM allows for engineering polymers.